ACS APPLIED MATERIALS & INTERFACES

Research Article

www.acsami.org

Conjugated Oligomer-Based Fluorescent Nanoparticles as Functional Nanocarriers for Nucleic Acids Delivery

Xiaoyu Wang, Fang He,* Lingling Li, Hui Wang, Rongjian Yan, and Lidong Li*

State Key Lab for Advanced Metals and Materials, School of Materials Science and Engineering, University of Science and Technology Beijing, Beijing 100083, P. R. China

Supporting Information

ABSTRACT: Oligonucleotides such as siRNA and plasmid DNA (pDNA) have great potential for gene therapies. Multifunctional, environment-resistant carriers with imaging capabilities are required to track the assembly and disassembly of oligonucleotides, monitor the delivery processes, and develop new delivery systems. Conjugated polymers and oligomers can potentially be used as novel materials for functional nanocarriers with both delivery and imaging abilities. In this work, a novel π-conjugated oligomer 4,7-(9,9′-bis(6-adenine hexyl)fluorenyl)-2,1,3-benzothiadiazole (OFBT-A) modified with nucleotide adenine (A) groups in its side chains is synthesized and characterized. Fluorescent nanoparticles based on the π-conjugated oligomers OFBT-A are developed as novel functional nanocarriers for oligonucleotides. Single-stranded DNA (ssDNA) TR-T5 labeled with Texas Red (TR) fluorescent dye is selected as a model payload oligonucleotide. The capture abilities and stability of OFBT-A are investigated by monitoring the fluorescence resonance energy transfer (FRET) efficiency between the OFBT-A nanoparticles and TR labels in solution. The OFBT-A/TR-T5 composites are stable in solution at high ionic strengths (0−500 mM) and have a wide working pH range, from 3.0 to 9.5. The in vitro profile demonstrates that the release of the TR-DNA is induced by the ssDNA A43, which has a high charge density. The release process is monitored by measuring the changes in FRET efficiency and fluorescence color for the OFBT-A/TR-T5 composites. Using this carrier, the uptake of TR-DNA by A549 lung cancer cells is observed. Both the OFBT-A nanoparticles and the OFBT-A/TR-T5 composites show high cytocompatibility. We anticipate that these novel functional nanocarriers will provide a safe strategy for monitoring the gene delivery process.

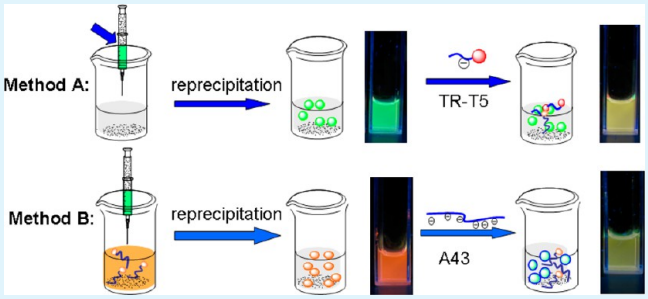

KEYWORDS: *fluorescence, conjugated oligomers, nanoparticles, fluorescence resonance energy transfer, delivery, nanocarrier*

INTRODUCTION

Gene therapy can be used for the treatment of a wide variety of diseases, including cancer, neurodegenerative diseases, antiviral disease, hematological diseases, and hereditary genetic disorders.[1−4] However, the highly negatively charged phosphodiesters on the oligonucleotides' backbone prevents their internalization into the cell membranes. Moreover, the naked oligonucleotides are subject to adverse biological interactions such as enzymatic degradation or immune stimulation in biological media. Therefore, to allow therapies to be successfully applied, the genes must typically be conjugated with or encapsulated by nanocarriers, to allow effective delivery and to prevent degradation. The impact of targets and safe carriers on short oligonucleotides such as small interfering RNA (siRNA) is especially pronounced because of their powerful ability to knock down pathogenic genes.[5−9]

Several short oligonucleotide carriers have been established during the past decade. Viral vectors are typically seen as highly risky because of their immunogenic and mutagenic toxicity; therefore, nonviral carriers based on polymers, liposomes, nanohydrogels, and silica nanoparticles have been investigated extensively.[10−20] Recently, multifunctional nanocarriers loaded with fluorescent molecules with imaging capabilities have been explored for tracking the assembly and disassembly of oligonucleotides, monitoring the delivery processes, and further developing new delivery systems.[21,22] Typical fluorescent imaging agents include organic fluorescent molecules and semiconductor quantum dots (QDs). Light-harvesting conjugated polymers (CPs) have gained much attention as fluorescent probes because of their "molecule-wire" effect, which can amplify the signals from small organic dyes via fluorescence resonance energy transfer (FRET); these polymers have been widely applied in highly sensitive chemical and biological sensors.[23−31] Recently, nanoparticles manufactured from CPs or π-conjugated oligomers with unique properties such as high fluorescence brightness, high two-photon excitation cross sections, good photostability, and low cytotoxicity have emerged as novel fluorescent probes for cellular imaging and sensing.[32−44] Because of their excellent properties, CPs have been proposed as novel materials to serve

Received: March 28, 2013
Accepted: May 30, 2013
Published: May 30, 2013

as functional nanocarriers with both delivery and imaging abilities. However, although different kinds of polymers have been developed for drug and gene carriers, nanocarriers based on CPs have only rarely been investigated.[45−49]

The high positive charge of polymer nanocarriers often results in relatively high cellular toxicity. To mitigate these effects, hydrophobic moieties have been incorporated into the side chains of polymer carriers to improve the cytocompatibility.[50−52] In this study, we designed and synthesized novel π-conjugated fluorene oligomers 4,7-(9,9′-bis(6-adenine hexyl)-fluorenyl)-2,1,3-benzothiadiazole (OFBT-A) with the weakly hydrophilic nucleotide adenine (A) in the side chains. Short single-stranded DNA (ssDNA) labeled with Texas Red (TR) dye (named TR-T5) could be efficiently loaded into the OFBT-A nanoparticles in the reprecipitation process. The stability of the nanocomposites and the release of TR-T5 were investigated by measuring the FRET between the OFBT-A and the Texas Red (TR) dye labels on the DNA. We demonstrated that this nanosystem could be rapidly ingested by cancer cells and that it had low cytotoxicity. This unique nanocarrier system provides a new avenue for the development of functional gene delivery systems for fluorescent tracking.

EXPERIMENTAL SECTION

Materials and Measurements. Adenine was obtained from Alfa Aesar. Tetrakis(triphenylphosphine)palladium(0) ($Pd(PPh_3)_4$) was purchased from Acros. All other chemicals were obtained from Beijing Chemical Co. and were used without further purification, unless otherwise noted. Compounds 2-bromo-9,9-bis(6-bromohexyl)-fluorene (**1**)[53] and 4,7-bis(4,4,5,5-tetramethyl-1,3,2-dioxaborolane)-2,1,3-benzothiadiazole (**3**)[54]were synthesized according to reported procedures. All of the oligonucleotides were purchased from Shanghai Sangon (Shanghai, China). The DNA concentrations were determined by measuring the absorbance at 260 nm. The ^{1}H-NMR and ^{13}C-NMR spectra were recorded on a 400 MHz AC Bruker spectrometer. MALDI-TOF mass spectra were obtained using a Bruker Biflex MALDI-TOF spectrometer. UV-Vis absorption spectra were collected on a Hitachi U3900 spectrophotometer. Fluorescence spectra data were obtained using a Hitachi F-7000 fluorescence spectrometer equipped with a Xenon lamp excitation source at room temperature. The SEM images were recorded using a JSM-7401F high-resolution field emission scanning electron microscope. The zeta-potential and average hydrodynamic diameters of the nanoparticles were measured using a Nano ZS90 instrument (Malvern Instrument Ltd., England) in dilute solutions at room temperature. Fluorescence images of cells were recorded using an Olympus FV1000-IX81 confocal laser scanning biological microscope, with 405 and 559 nm excitation. Flow cytometric analysis was obtained by BD FACSCalibur (Becton, Dickinson and Company, USA). Electrophoresis analysis experiments were obtained by loading OFBT-A nanoparticles, OFBT-A/TR-T5 nanocomposites, and OFBT-A onto a 15% nondenaturing polyacrylamide gel in a 1× TBE buffer (8.9 mM tris base, 8.9 mM boric acid, 0.2 mM EDTA, pH 7.9) with a voltage of 100 V for 15 min. A photograph was taken in a WD-9403F UV device under 365 nm UV light.

Synthesis of 2-Bromo-9,9-bis(6′-(adenine)hexyl) Fluorene (2). NaH (685 mg, 20 mmol) was added to a mixture of adenine (2.70 g, 20 mmol) in dry DMF (40 mL). After stirring for 2 h at room temperature, the compound **1** (5.40 g, 40 mmol) in DMF (15 mL) was added dropwise. The resulting mixture was stirred at 110°C overnight. After the removal of the solvent under reduced pressure, the residue was extracted using $CHCl_3$, and the combined organic layers were washed using an aqueous HCl solution and water and then dried over anhydrous $MgSO_4$. The solvent was then removed, and the residue was purified via silica gel column chromatography using CH_2Cl_2/methanol (v/v = 15:1) to yield **2** (1.87g, 29%) as a light yellow solid. ^{1}H NMR ($CDCl_3$, 400 MHz), δ (ppm): 8.32 (s, 2H), 7.69 (s, 2H), 7.64−7.66 (d, 1H), 7.45−7.53 (d, 1H), 7.41−7.45 (t, 2H), 7.26−7.32 (m, 3H), 4.04−4.08 (t, 4H), 1.87−1.90 (t, 4H), 1.68 (s, 4H), 1.08 (s, 8H), 0.55 (s, 4H).^{13}C NMR (CDCl3, 400 MHz), δ(ppm): 155.5, 152.9, 152.5, 150.1, 149.8, 140.4, 140.1, 140.0, 130.1, 127.6, 127.1, 125.9, 122.7, 121.1, 121.0, 119.8, 119.6, 55.1, 43.7, 40.0, 29.8, 19.1, 26.1, 23.3. MS (MALDI-TOF) *m*/*z*: 676.28 (M^+).

Synthesis of OFBT-A. Monomer 2 (678 mg, 1 mmol) and monomer 3 (194 mg, 0.5 mmol) were dissolved in 32 mL of toluene, and then 8 mL of 2.0 M potassium carbonate was added. After degassing with nitrogen for 30 min, 10 mg of the catalyst $Pd(PPh_3)_4$ was added. The mixture was stirred at 80°C for 60 h, under nitrogen. The obtained solution was cooled and extracted with CH_2Cl_2. The organic layer was combined and dried over anhydrous $MgSO_4$. The solvent was then removed, and the residue was purified using column chromatography on silica gel with CH_2Cl_2/methanol (*v*/*v* = 10:1) as the eluent, giving a yellow solid (200 mg, 21%). ^{1}H NMR ($CDCl_3$, 400 MHz), δ (ppm): 8.29−8.32 (d, 4H), 7.81−7.98 (m, 2H), 7.71−7.39 (s, 4H), 7.61−7.63 (d, 2H), 7.51−7.53 (d, 2H), 7.38−7.43 (m, 4H), 7.27−7.32 (m, 6H), 5.71 (s, 8H), 4.02−4.05 (t, 8H), 1.83−1.89 (m, 8H), 1.66 (s, 8H), 1.05 (s, 16H), 0.51 (s, 8H). ^{13}C NMR ($CDCl_3$, 400 MHz), δ(ppm): 155.6, 155.4, 152.9, 152.5, 150.0, 149.8, 140.3, 140.1, 139.9, 130.1, 127.6, 127.1, 126.0, 122.8, 121.2, 121.0, 119.8, 119.6, 55.2, 43.8, 40.1, 29.8, 29.3, 26.1, 23.7. MS (MALDI-TOF) *m*/*z*: 1336.7 (M^+).

Preparation of Nanocomposites. All of the nanocomposites were prepared using the precipitation technique. OFBT-A was first dissolved in a THF solution (1×10^{-3} M). 10 μL of the THF solution of OFBT-A was rapidly injected into 1 mL of water to obtain OFBT-A nanoparticles. To investigate the assembly process of the OFBT-A nanoparticles, samples were prepared by adding 10 μL of the OFBT-A in THF (1×10^{-3} M) stock solution to the THF/H_2O mixtures with various water fractions (THF/H_2O = 100%THF, 90%/10%, 80%/20%, 70%/30%, 60%/40%, 40%/60%, 30%/70%, 20%/80%, 100% H_2O in volume). Different concentrations of TR-T5 were then added to the OFBT-A nanoparticle solution, giving OFBT-A&TR-T5 complexes. 10 μL of the THF solution of OFBT-A was rapidly injected into 1 mL of the solutions containing different concentrations of TR-T5, TR-R5, TR-T8, TR-T11, and TR-T20, to obtain OFBT-A/TR-T5, OFBT-A/TR-R5, OFBT-A/TR-T8, OFBT-A/TR-T11, and OFBT-A/TR-T20 nanocomposites, respectively.

Characterization of Nanocomposites. The size and morphology of the nanocomposites were investigated using scanning electron microscopy (SEM, JEOL JSM-7401F). SEM samples were prepared by dropping the nanoparticle suspension onto silicon wafers and drying them at room temperature. To enhance the contrast and quality of the SEM images, the prepared samples were sputter-coated with gold. The hydrodynamic diameter and zeta potential of the nanocomposites were measured in aqueous solutions using a DLS instrument (Malvern Zetasizer Nano ZS90). UV-Vis absorption spectra were measured for the nanocomposites in solution, using a Hitachi U3900 spectrophotometer in the range of 220−700 nm. Fluorescence spectra data were obtained using a Hitachi F-7000 fluorescence spectrometer equipped with a Xenon lamp excitation source at room temperature. The emissions from OFBT-A and TR were examined using excitation at 310 and 580 nm, respectively. The fluorescence photographs were taken under a UV lamp using 365 nm excitation.

Stability Assay of the Nanocomposites. To study the influence of ionic strength in the NP system, 0−100 μL of NaCl (5 M) solution was added to the water to adjust the ionic strength. Then, 3 μL of TR-T5 (5×10^{-5} M) was added to 1 mL of the NaCl solution, and 10 μL of OFBT-A in THF (1×10^{-3} M) was subsequently added to the solution rapidly to form the nanocomposites. Fluorescent spectra were then measured using excitation at 310 nm.

1 mL of TR-T5 (1.5×10^{-7} M) in PBS buffer solution (10 mM, pH = 7.4) was added to six quartz cuvettes, and 10 μL of the OFBT-A stock solution in THF (1×10^{-3} M) was rapidly added to each solution to form the nanocomposites. To investigate the influence of the pH on the nanocomposites, the pH of the six mixtures was adjusted to 3.0, 5.0, 6.0, 7.4, 8.0, and 9.5, via the addition of HCl (1 M) or NaOH (1 M) solutions.

TR-T5 Release from Nanocomposites. 1 mL of TR-T5 (1.5×10^{-7} M) in water was added to six quartz cuvettes, and 10 μL of the OFBT-A stock solution in THF (1×10^{-3} M) was rapidly added to each cuvette to form the nanocomposites. Then, 0, 1, 5, 10, 20, 45, and 90 μL of A43 (1×10^{-4} M) was added to the solution and left to sit for 1 h. The fluorescent spectra were measured for the six samples at 0 min, 2 min, 5 min, 10 min, 30 min, and 1 h, using excitation at 310 nm.

Cellular Imaging for Nanoparticles (NPs). A549 cells were grown in DMEM medium containing 10% fetal calf serum (FBS) (v/v), and 160 000 cells were then seeded on 35 × 35 mm culture plates and incubated at 37°C in a 5% CO_2 humidified atmosphere for 24 h. 150 μL of OFBT-A/TR-T5 nanocomposites were added to 850 μL of the medium containing A549 cells in a 35 × 35 mm plate (final concentration: (OFBT-A) = 1.5×10^{-6} M, (TR-T5) = 2.25×10^{-8} M). At the same time, 150 μL of OFBT-A nanoparticles ((OFBT-A) = 1×10^{-5} M) alone and 150 μL of TR-T5 ((TR-T5) = 1.5×10^{-7} M) alone were added to 850 μL of medium containing A549 cells in two different 35 × 35 mm plates. After incubation at 37 °C for 10 min, 4 h, and 12 h, the medium was removed, and the cells were washed once using phosphate buffered saline (PBS, pH 7.4) and fixed for 20 min in PBS containing 4% formaldehyde. After another two PBS washing steps, the specimens were then observed using an oil immersion lens (100× magnification; NA 1.4) in an Olympus FV1000-IX81 confocal laser scanning microscope, using a DM405/488/559 dichroic mirror, and capturing within a bandwidth of 460−560 nm for the 405 scan or 520−620 nm for the 559 scan. Images were recorded at 512 × 512 12-bit, resulting in a total image size width and height of 127 μm × 127 μm. OFBT-A was examined using a 405 nm laser and is highlighted in green; TR-T5 was examined using a 559 nm laser and is highlighted in red. Moreover, then the fluorescence spectra in A549 cells incubated by OFBT-A/TR-T5 nanocomposition for 4 h were determined in XYL spectrum scanning mode from 420 nm to 650 nm with a 405 nm laser (resolution = 15 nm, step size = 2 nm).

Flow Cytometry Experiment. A549 cells were incubated by OFBT-A/TR-T5 composites for 4 h in the same condition of the cellular imaging experiments. Then, the cells were washed twice with PBS buffer (pH 7.4), digested by trypsin for 5 min at room temperature, and centrifuged at 1000 rpm for 5 min. The cell pellets were dispersed in 1 mL of PBS buffer. Detected signals were recorded in Channel FL2-H using a 488 nm laser. The flow cytometry diagrams were obtained from a population of 3×10^4 cells.

In Vitro Cell Viability Assay Using the MTT Method. A549 cells were seeded in 96-well tissue culture plates and maintained overnight in DMEM medium containing 10% FBS (v/v) and then treated using various concentrations of OFBT-A nanoparticles (0−4.5 μM) and OFBT-A/TR-T5 nanocomposites (0−4.5 μM) at 37°C for 24 h. The concentration of OFBT-A/TR-T5 nanocomposites was determined using the OFBT-A, and the concentration ratio ((OFBT-A)/(TR-T5)) was maintained at a constant 100. Subsequently, 100 μL of 3-(4,5-dimethylthiazol-2-yl)-2,5-diphenyltetrazolium bromide (MTT, 1 mg/mL in PBS) was added to each well after the medium was removed, and this was followed by incubation at 37 °C for 4 h. The supernatant was removed, and the cells were lysed by adding 100 μL of DMSO per well. After shaking for 5 min, the absorbance of the purple formazan at 490 nm was studied using a Spectra MAX 340PC plate reader.

RESULTS AND DISCUSSION

Synthesis and Characterization of Oligomer OFBT-A. The employed oligomer OFBT-A is a fluorene oligomer that consists of a π-conjugated core formed from two fluorene units connected by a 2,1,3,-benzothiadiazole (BT) linker. The oligomer OFBT-A was obtained via the Suzuki coupling of monomer 2-bromofluorene with 2,1,3,-benzothiadiazole boronic ester in a 21% yield, which was performed according to the synthesis route shown in Figure 1a. The weakly hydrophilic moiety nucleotide adenine was covalently linked to the side chains of the fluorene units. The oligomers could perfectly

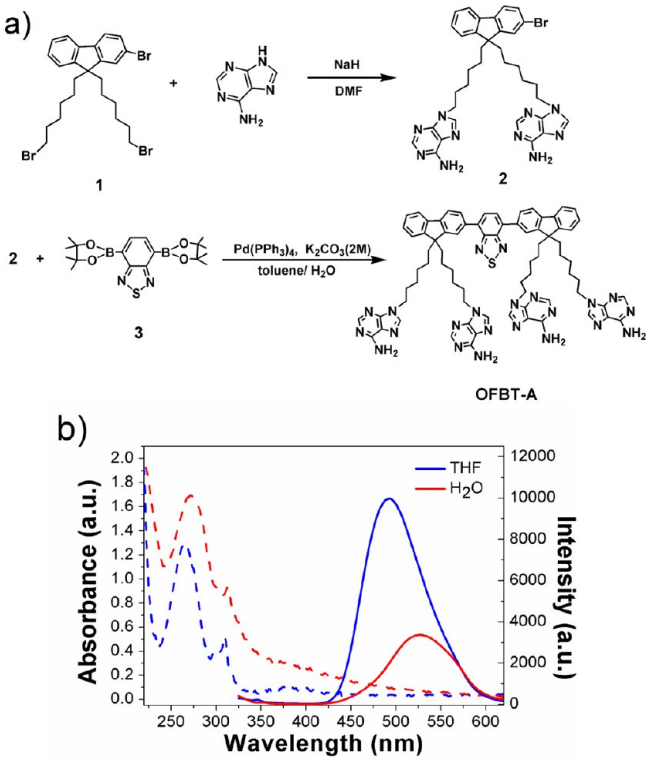

Figure 1. (a) Chemical structure of oligomer OFBT-A, and the synthesis route for the OFBT-A oligomers; (b) UV-Vis absorption (dashed line) and emission spectra (solid line) for OFBT-A in THF and H_2O. The concentration of OFBT-A was 3×10^{-5} M for the absorption spectra and 1×10^{-6} M for the emission spectra. The excitation wavelength was 310 nm.

dissolve in nonpolar solvents such as $CHCl_3$ and THF and had very low solubility in CH_3OH and H_2O.

Then, OFBT-A nanoparticles were prepared using the reprecipitation method, via the rapid addition of 10 μL of a 1 mM water-miscible THF stock solution to 1 mL of water. In this way, the nanoparticles can be formed by the self-assembly of oligomers in the aqueous solution. The photophysical properties of OFBT-A were investigated in THF and H_2O. As shown in Figure 1b, the UV-Vis absorption spectra of OFBT-A both in THF and in H_2O showed the absorbance of the fluorene units at 312 nm, the BT units at 385 nm, and the adenine at 260 nm. However, the emission spectra only showed an emission peak for the BT units at approximately 492 nm; no obvious emission peak was observed for the fluorene units. The results indicated that an efficient intramolecular energy transfer occurred from fluorene to BT, similar to the results reported previously for fluorene-*co*-2,1,3,-benzothiadiazole derivatives.[37,55−58]

Moreover, the absorbance of the OFBT-A was enhanced, but the absorption peaks were slightly shifted in H_2O. However, the emission peak was red-shifted by approximately 33 nm, and the emission intensity of the oligomers in H_2O was quenched by approximately 70% compared with the intensity in THF. Then, to obtain a better understanding of the self-assembly of OFBT-A, we studied the emission spectra of OFBT-A in 1 mL solutions with different ratios of THF/H_2O (v/v). The results showed that, in the solutions containing more than 30% THF, the emission intensity was gradually increased with the increase of the ratios of THF/H_2O compared with the intensity of OFBT-A in pure water. The emission peak was blue-shifted

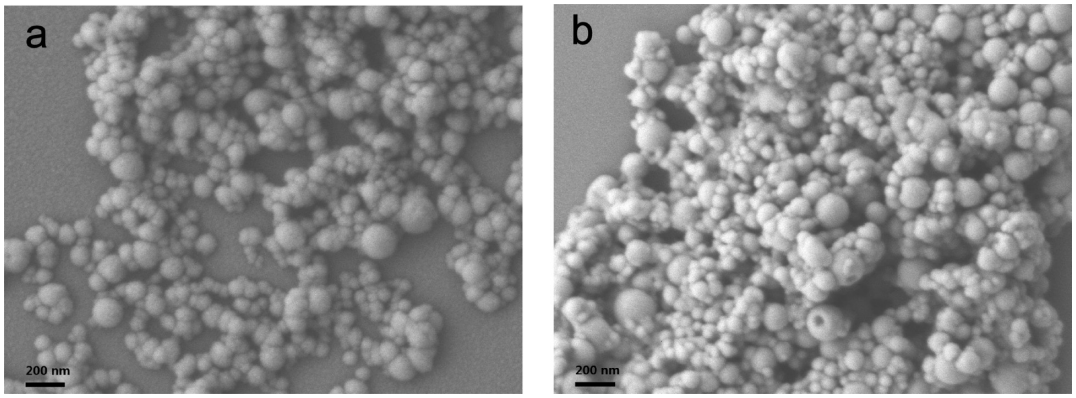

Figure 2. SEM images of (a) OFBT-A nanoparticles and (b) OFBT-A/TR-T5 composites. The scale bar represents 200 nm.

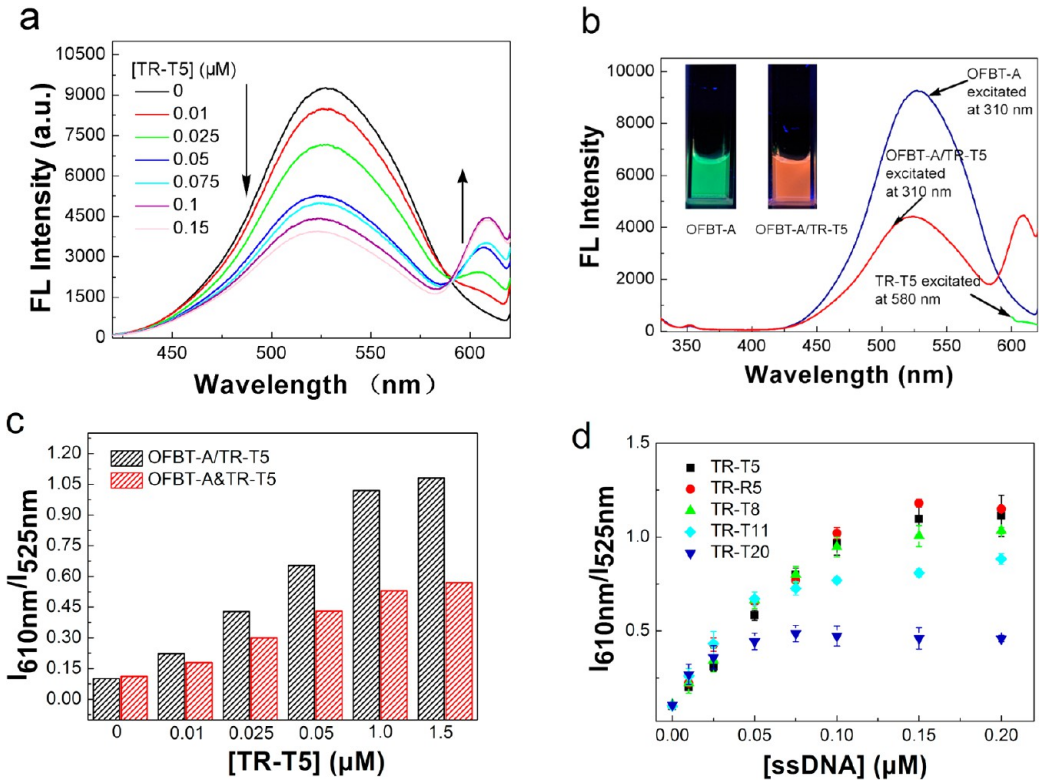

Figure 3. (a) Emission spectra for the OFBT-A/TR-T5 nanocomposites after co-reprecipitation with different concentrations of TR-T5 in H_2O, (TR-T5) = 0–1.5 × 10^{-7} M; (b) emission spectra for OFBT-A nanoparticles, OFBT-A/TR-T5 nanocomposites, and TR-T5 in H_2O, (TR-T5) = 1.5 × 10^{-7} M; (c) the FRET ratio $I_{610\ nm}/I_{525\ nm}$ for OFBT-A&TR-T5 and OFBT-A/TR-T5, which were prepared using methods A and B, respectively, (TR-T5) = 0–1.5 × 10^{-7} M; (d) the FRET ratio $I_{610\ nm}/I_{525\ nm}$ as a function of the concentration of ssDNAs TR-T5, TR-R5, TR-T8, TR-T11, and TR-20, (ssDNAs) = 0–2.0 × 10^{-7} M. The excitation wavelength was 310 nm. (OFBT-A) = 1 × 10^{-5} M in all figures.

(Figure S1 in the Supporting Information). In contrast, the emission peak of OFBT-A red-shifted and was quenched further in the solution containing less than 30% THF. Previous studies revealed that the BT emission was sensitive to the aggregation of the materials and the polarity of the environment in terms of its charge transfer electronic states; in more hydrophilic environments, a red-shift and a decrease in the fluorescence intensity were observed.[58−60] The emission results illustrated that the OFBT-A formed loosely aggregated nanoparticles in H_2O (because of the weakly hydrophilic adenine side chains), which offered space for the encapsulation of DNA.

The SEM images in Figure 2a confirmed that the resulting particles were approximately spherical in shape, with an average size of 88.6 ± 15 nm. The ζ potential measurements on the nanoparticles in the aqueous solution gave a value of 26.6 ± 1.0 mV, which was consistent with the high abilities of the nanoparticles for internalization into cells and the loading of negatively charged DNA/RNA. The nanoparticles were stabilized in the aqueous solution by the electrostatic repulsion between them, which resulted from their same-sign surface charges. Dynamic light scatting (DLS) measurements showed a similar average hydrodynamic radius of 86.7 ± 3.5 nm, with a polydispersity index (PDI) of 0.136, illustrating the good dispersibility of the nanoparticles in solution.

Oligonucleotide Loading Ability of the OFBT-A Nanoparticles. The ability of the OFBT-A nanoparticles to capture oligonucleotides was investigated. TR-T5 ssDNA

dx.doi.org/10.1021/am401118r | ACS Appl. Mater. Interfaces 2013, 5, 5700−5708

(sequence shown in Scheme 2) labeled with fluorescent Texas Red dye was selected as a model oligonucleotide. The emission spectrum of the OFBT-A nanoparticles showed a good overlap with the absorption spectrum of TR (Figure S2a in the Supporting Information). Efficient FRET could therefore occur via the Förster mechanism.[61] As shown in Figure 3a, when 10 μL of an OFBT-A solution in THF was added to 1 mL of water containing different concentrations of TR-T5 (Method B in Scheme 1), the emission from OFBT-A (at 525 nm) was

Scheme 1. Schematic Illustration of the Different Sample Preparation Methods and the Mechanism of Capture and Release

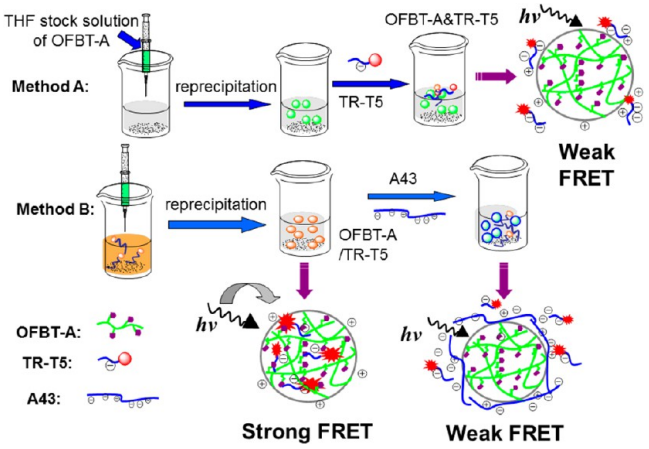

gradually quenched as the increase of TR-T5 concentration, while the intensity of the TR emission (at 610 nm) gradually increased. These results indicated that an efficient energy transfer from OFBT-A to TR occurred. From the absorption spectra and fluorescence excitation of the OFBT-A/TR-T5 composites (shown in Figure S2b in the Supporting Information), we observed that the dominant absorption peaks for the nanocomposites were due to OFBT-A, whereas only a relatively weak absorption can be measured from the TR for their relative low concentration. With excitation at 310 nm, where TR has no absorption, the direct emission from the TR acceptor dye was minimized. However, through the intramolecular energy transfer from OFBT-A, and the intraparticle energy transfer from OFBT-A to the TR, the emission intensity of TR was amplified approximately 12-fold under excitation at 310 nm compared with the intensity measured for TR that was directly excited at 580 nm. The color of the nanocomposites changed from green to orange-red under UV light with a wavelength of 365 nm (Figure 3b).

The SEM image of the nanocomposites illustrated that spherical nanoparticles with diameters of approximately 94.1 ± 18 nm were obtained (Figure 2b); the presence of TR-T5 had only a small effect on the particle size and morphology. The ζ potential of the nanocomposites decreased from 26.6 ± 1.0 to −7.1 ± 2.0 mV after the loading of the TR-T5 (Table S1 in the Supporting Information). The TR-T5 loading reduced the surface charge of the nanoparticles to close to neutral (the zeta potential ranged between −10 and +10 mV); a minimal surface charge can minimize phagocytosis and immunological reactions in vivo.[62,63]

To determine whether the DNA was located primarily within the nanoparticles or free in solution, a corresponding experiment was performed as follows: 10 μL of an OFBT-A solution in THF was added to 1 mL of pure water, and different quantities of TR-T5 were added to the solution (OFBT-A&TR-T5 prepared using Method A shown in Scheme 1). The FRET efficiency between the OFBT-A nanoparticles and the free TR-T5 was then examined. FRET between OFBT-A and TR was also observed in this system because a few negatively charged TR-T5 attached on the surface of the OFBT-A nanoparticles through electrostatic interactions. However, from the FRET ratio ($I_{610\ nm}/I_{525\ nm}$) of OFBT-A and TR-T5, much lower FRET efficiencies were observed in OFBT-A&TR-T5 compositions than that of in OFBT-A/TR-T5 nanocomposites, and the FRET ratio interval of these two compositions increased as the increase of TR-T5 concentrations (Figure 3c). Moreover, the ζ potential of this system decreased only slightly from 26.6 ± 1.0 to 16.7 ± 3.2 mV after a few negatively charged TR-T5 molecules became attached on the surface of the nanoparticles. These results indicated that TR-T5 was loaded into the matrix of the OFBT-A nanoparticles in the OFBT-A/TR-T5 nanocomposites, resulting in more efficient FRET and a larger decrease in the zeta potential compared with the OFBT-A&TR-T5 composites.

The sequence of TR-T5 contained only thymine (T) nucleotides, which were complemented by the A nucleotides in OFBT-A; the capability of the nanoparticles to capture oligonucleotides with noncomplementary bases was also studied. TR-R5 ssDNA without T nucleotides was coprecipitated with OFBT-A, and the FRET efficiency was studied. As shown in Figure 3d, the FRET ratio ($I_{610\ nm}/I_{525\ nm}$) for OFBT-A/TR-R5 was similar to the ratio measured for OFBT-A/TR-T5. Efficient FRET was also observed for the OFBT-A/TR-R5 complexes. The nanoparticles could capture oligonucleotides with different sequences without selectivity. The nonspecific hydrogen-bond interactions between the nucleotides also can result in the efficient loading of the DNA. The results illustrated that the decrease in the FRET efficiency could be used as an indicator for the release of the oligonucleotides.

To evaluate the capture ability of the OFBT-A nanoparticles, direct evidences are provided by electrophoresis analysis using a 15% nondenaturing polyacrylamide gel. The gel was not stained, and the visible bands come from the fluorescence of OFBT-A and TR. The gel image displayed in Figure S3 in the Supporting Information clearly proves the efficient loading of TR-T5 in OFBT-A nanoparticles by monitoring the intensity of the bands of TR-T5. It shows that the intensity of TR-T5 band obviously decreases gradually in the OFBT-A/TR-T5 compositions with increase of OFBT-A concentrations in lanes 2−6 compared with the TR-T5 alone in lane 7. The result in lane 6 demonstrated that almost all of the TR-T5 were loaded into the OFBT-A nanoparticles in the same condition as the emission spectra in Figure 3b.

In addition, emission spectra were measured for the OFBT-A nanoparticles after the loading of ssDNA with different charge densities (different lengths and concentrations). TR-labeled ssDNAs TR-T8, TR-T11, and TR-T20, with 8, 11, and 20 bases, respectively, were selected. The sequences of the ssDNAs are shown in Scheme 2. As shown in Figure 3d, the FRET ratio ($I_{610\ nm}/I_{525}$nm) increased as the DNA concentration was increased, and it reached a plateau when the ratio of OFBT-A unit and DNA charge was approximately 10:1. The maximum FRET ratio ($I_{610\ nm}/I_{525}$nm) of OFBT-A/ssDNAs decreased compared with OFBT-A/TR-T5 nanocompositions while the ssDNAs with length up to 11 nucleotides further decreased to 0.37 at TR-T20, which illustrated less long chain DNA was

dx.doi.org/10.1021/am401118r | ACS Appl. Mater. Interfaces 2013, 5, 5700−5708

Scheme 2. Sequences of the ssDNAs Used in the Experiments

TR-T5: 5'-Texas Red-TTTTT-3'
TR-R5: 5'-Texas Red-CGGAG-3'
TR-T8: 5'-Texas Red-TTTTTTTT-3'
TR-T11: 5'-Texas Red-CATGTATTTTT-3'
TR-T20: 5'-Texas Red-CATGGAGCACATGTATTTTT-3'
A43: 5'-CTGGCCTCCGATCTCATACCTTCTTTCCGCATCGAGCACATGT-3'

loading in the nanoparticles. The DLS measurements showed that the OFBT-A/TR-T8, OFBT-A/TR-T11, and OFBT-A/TR-T20 nanocomposites had hydrodynamic diameters (approximately 120 nm) and low PDIs that were similar to those of OFBT-A/TR-T5, and the zeta potential of the nanocomposites also showed only a small decrease compared with OFBT-A/TR-T5 (Table S1 in the Supporting Information). We therefore propose that the capturing abilities of the nanoparticles were correlated with the charge density of the DNA. Less TR-T20 chains with more charge, that is less TR, were loaded into the nanoparticles than in the TR-T5 case, causing the lower FRET efficiency.

Stability of the OFBT-A/DNA Nanocomposites, and DNA Release from the Nanocomposites. While TR-T5 ssDNA was loaded into the OFBT-A nanoparticles, the stability of the nanocomposites was investigated in different environments for their further application in in vitro or in vivo systems. While biological solutions with high salt concentrations and electrostatic interactions are sensitive to the ionic strength, the FRET of the nanocomposites was investigated in solutions with different ionic strengths. As shown in Figure 4a, only a small degree of quenching was observed in the fluorescence, and the FRET efficiency changed only slightly as the ion strength was varied from 0 to 500 mM. The DLS experiments illustrated that the hydrodynamic diameters and PDIs of the nanocompositions also only have little effect by the ionic strength of the solutions (Table S2 in the Supporting Information). Moreover, to determine the working pH range for the OFBT-A/TR-T5 nanocomposites, the effects of the medium pH values on the FRET efficiency of OFBT-A and TR-T5 were investigated in phosphate buffer (PBS, 10 mM). As shown in Figure 4b, the emission spectra also changed only slightly over the pH range from 5.0 to 9.5. A quenching of only approximately 20% was exhibited at pH 3.0. The FRET efficiency of the nanoparticles was stable under the different solution conditions studied here.

In this system, we found that the FRET efficiency of OFBT-A/TR-T5 was decreased by the presence of DNA with a high charge density. Emission spectra were measured for the OFBT-A/TR-T5 nanocomposites after the addition of different concentrations of ssDNA A43 (with 43 bases; the sequence of A43 is shown in Scheme 2). As shown in Figure 5a, the emission intensity for TR (at 610 nm) gradually decreased, and the intensity for OFBT-A (at 525 nm) gradually increased as the concentration of A43 was increased in the solutions. The decrease of the FRET efficiency could be used as an indicator for the release of the oligonucleotides, as shown by the results detailed above, and we believe that the gradual decrease in the FRET efficiency corresponded to the gradual release of TR-T5. To further demonstrate this, we also investigated the FRET efficiency of OFBT-A/TR-T5 as a function of time after the addition of different concentrations of A43. Figure 5b shows the FRET ratios ($I_{610\ nm}/I_{525\ nm}$) for OFBT-A/TR-T5 in the presence of different concentrations of A43 as a function of time. At relatively low A43 concentrations, the FRET efficiency changed only slightly as a function of time. When the concentration of A43 was up to 10 times that of TR-T5, the balance of the nanocomposites was destroyed, and the FRET efficiency gradually decreased. The FRET ratio ($I_{610\ nm}/I_{525\ nm}$) decreased to 0.5 when the concentration of A43 was 60 times that of TR-T5. It is likely that the short TR-T5 was repelled by the strongly negative charge density of the A43 in this environment. While there were many nucleotides in the cellular system, the release of DNA was feasible in the cells. Moreover, the nanocomposites exhibited different fluorescent colors as the TR-T5 was released (Figure 5c). These nanocomposites show good potential for applications in gene delivery research.

Cellular Internalization Assay and Cell Viability Assay. Another important question to be answered was whether the nanocomposites could be taken up by cells after the DNA was loaded. Motivated by this question, we incubated A549 lung cancer cells for 4 or 12 h with the OFBT-A nanoparticles alone, TR-T5 alone, or the OFBT-A/TR-T5 nanoparticles and subsequently investigated the cellular uptake using confocal laser scanning microscopy (CLSM). In the experiments, the localization of the OFBT-A nanoparticles and the TR-T5 was investigated by observing each channel for the detected fluorescence derived from each laser excitation separately. The fluorescence of the OFBT-A nanoparticles was visualized using excitation at 405 nm, and the TR was excited at 559 nm. Figure 6 shows confocal microscopy images of the A549 cells taken after incubation for 4 h. The OFBT-A nanoparticles alone showed a very weak cellular uptake as weak green fluorescence, but an increase in the uptake was observed after incubation for 12 h (Figure S4 in the Supporting Information). To exclude the

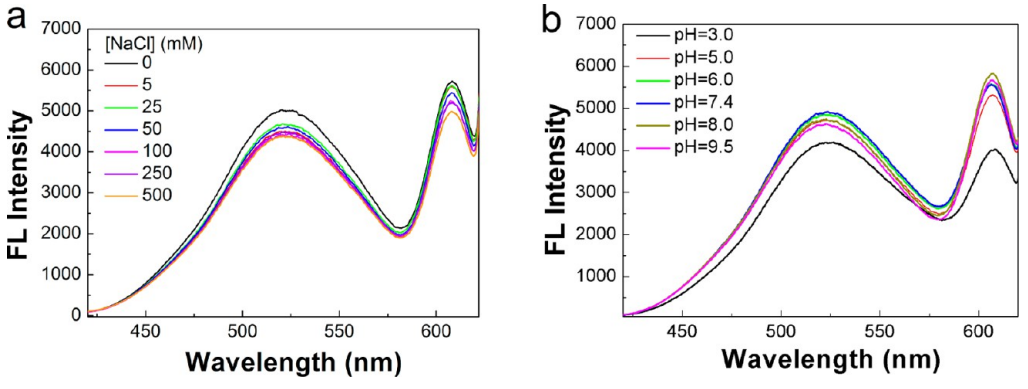

Figure 4. Emission spectra for OFBT-A/TR-T5 nanocomposites as a function of (a) different ionic strength, (NaCl) = 0−500 mM, and (b) different pH, (TR-T5) = 1.5×10^{-7} M, (OFBT-A) = 1×10^{-5} M. The excitation wavelength was 310 nm.

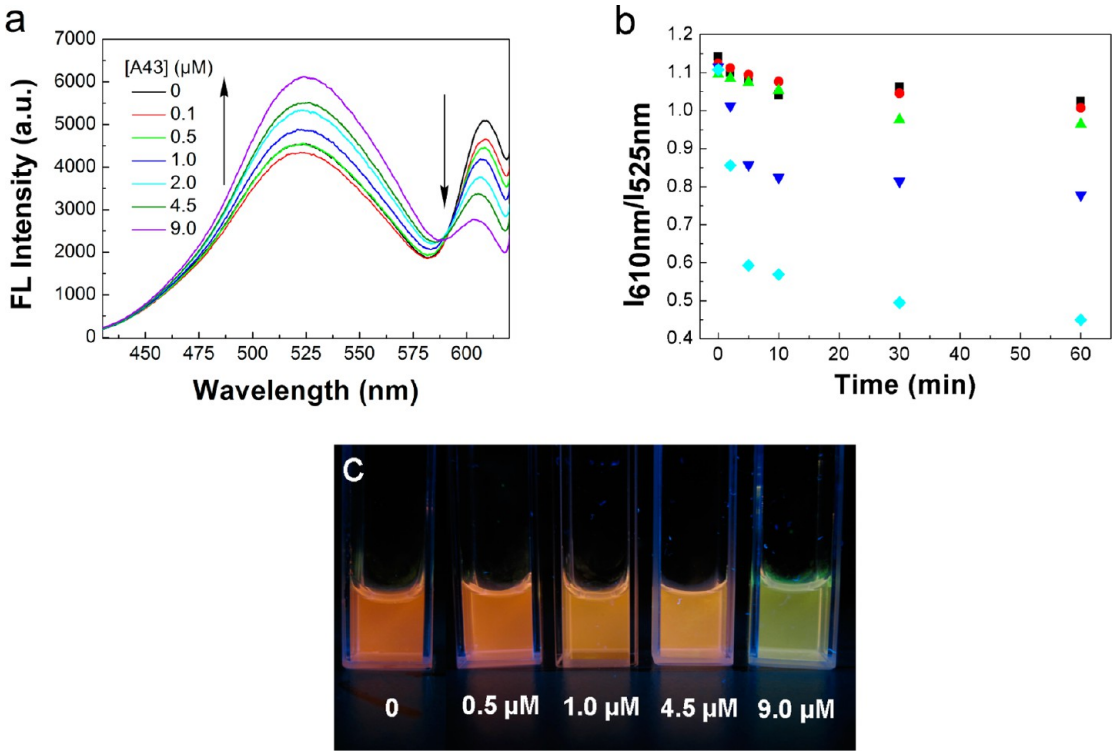

Figure 5. (a) Emission spectra for OFBT-A/TR-T5 nanocomposites with different concentrations of A43, (A43) = 0–9 × 10^{-6} M; (b) FRET ratio for OFBT-A/TR-T5 as a function time, in the presence of 0 μM (black ■), 0.5 μM (red ●), 1.0 μM (green ▲), 4.5 μM (blue ▼), and 9.0 μM (cyan ♦) of A43; (c) Fluorescence images of OFBT-A/TR-T5 under 365 nm UV light in the presence of 0, 0.5, 1.0, 4.5, and 9.0 μM of A43. (OFBT-A) = 1 × 10^{-5} M, (TR-T5) = 1.5 × 10^{-7} M. The excitation wavelength was 310 nm.

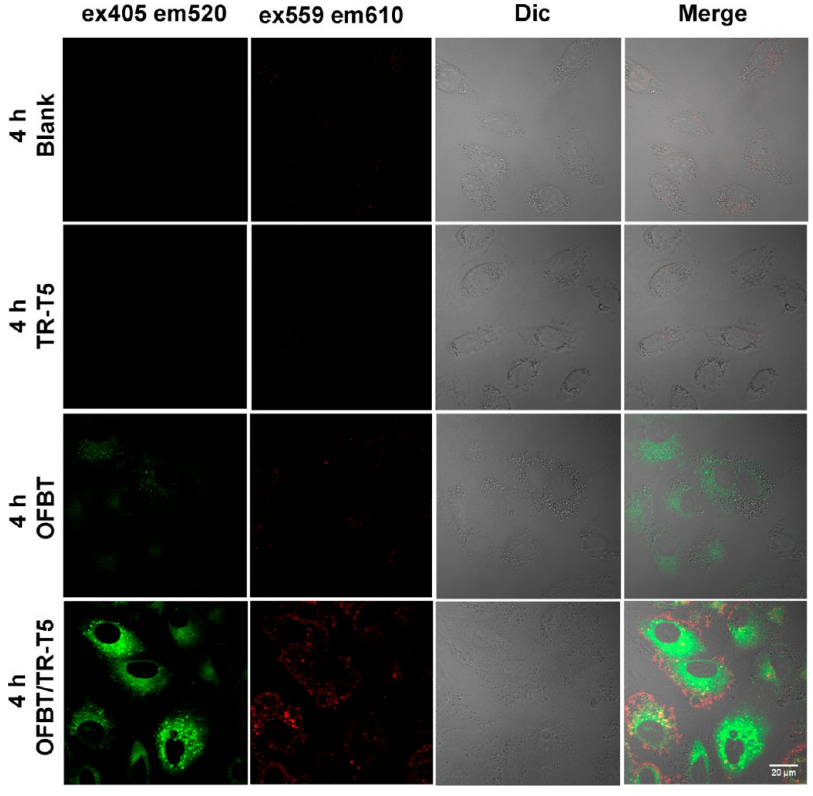

Figure 6. Fluorescent confocal microscopy images of A549 cells, which were either untreated or incubated for 4 h with OFBT-A nanoparticles alone, TR-T5 alone, or with OFBT-A/TR-T5 nanocomposites. The images were obtained using a 405 nm laser for OFBT-A (green) and a 559 nm laser for TR-T5 (Red). The scale bar represents 20 μm.

dx.doi.org/10.1021/am401118r | ACS Appl. Mater. Interfaces 2013, 5, 5700–5708

nonspecific uptake of TR-T5, we incubated the cells with TR-T5 alone. No obvious fluorescence was observed from the TR-T5 in the images after incubation for 4 or 12 h, similar to the blank assay. TR-T5 alone could not be internalized by the cells. For the OFBT-A/TR-T5 nanocomposites, strong fluorescence was observed from both TR and OFBT-A in the cytoplasm of the A549 cells after incubation for 4 h. A strong increase in the uptake was indicated by the increase observed in the green fluorescence signals, compared with the OFBT-A nanoparticles alone. The short DNA TR-T5 was delivered into the cells, as shown by the strong red fluorescence signals. Moreover, we also found that the OFBT-A/TR-T5 compositions can efficiently internalize into A549 cells after incubation only for 10 min, which illustrated the fast uptake rates of the nanocompositions. The nanoparticles cell uptake was further quantitatively determined by a flow cytometry experiment in the red channel. A549 cells incubation with OFBT-A/TR-T5 nanocompositions for 4 h illustrated a distinct peak shift with a positive percentage of 83.0%, after comparing with the negative A549 cells without stains (Figure S5 in the Supporting Information). The results clearly confirmed that the OFBT-A/TR-T5 nanocomposition was internalized by most of the cells.

Interestingly, in the overlap images in Figure 6 and enlarged images in Figure S6a in the Supporting Information, the green fluorescence from OFBT-A and red fluorescence from TR were clearly separated. The OFBT-A nanoparticles were internalized inside to the cytoplasm and near the nucleolus, but the location of the TR-T5 was mainly near the cellular member, maybe suggesting that the TR-T5 was released once the nanocomposition was internalized into the cell for the high quality of nucleic acid in the cytoplasm. The results demonstrated the release of TR-T5 in the cells. We also studied the emission spectra in the fluorescence range in cells to demonstrate it. As shown in Figure S6b in the Supporting Information, almost no FRET between OFBT-A and TR-T5 was observed in cell systems with excitation wavelength at 405 nm. Despite the fact that the limited loading abilities of the nanoparticles mean that real therapeutic genes such as siRNA could not be loaded into the cells in quantities high enough to provide sufficient knockdown efficiency, the results shown here demonstrate the high potential of these π-conjugated polymer nanoparticles for applications in gene research.

We also investigated the cytotoxicity of the OFBT-A alone and the OFBT-A/TR-T5 nanocomposites, using a 3-(4,5-dimethylthiazol-2-yl)-2,5-diphenyltetrazolium bromide (MTT) cell-viability assay. The absorbance of MTT at 490 nm is dependent on the degree of activation of the cells. The cell viability was thus expressed by the ratio of the absorbance of the cells incubated with various concentrations of OFBT-A nanoparticles and OFBT-A/TR-T5 nanocomposites to that of the cells incubated with culture medium only. As shown in Figure 7, the cell viability decreased to a much smaller degree after the A549 cells were incubated for 24 h with various concentrations of OFBT-A/TR-T5 (0–4.5 μM). In contrast, the cell viability was more than 92% when the concentration of OFBT-A was increased to 4.5 μM. The results indicated that both the OFBT-A nanoparticles and the OFBT-A/TR-T5 nanocomposites had low cytotoxicity. The cytocompatibility of OFBT-A was slightly enhanced after the loading of the DNA, which conferred a close-to-neutral neutral surface.

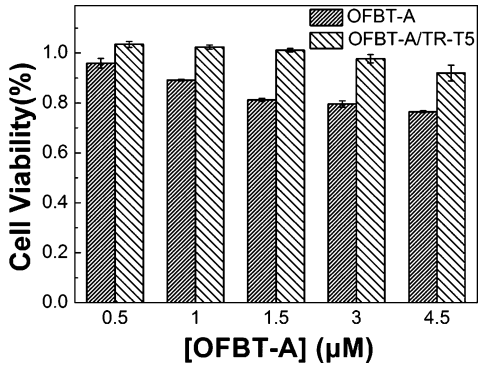

Figure 7. Cell viability results after the incubation of A549 cells with various concentrations of OFBT-A nanoparticles and OFBT-A/TR-T5 nanocomposites.

CONCLUSION

In this work, we designed and synthesized a novel π-conjugated oligomer OFBT-A with fluorene and 2,1,3,-benzothiadiazole units. The weakly hydrophilic nucleotide adenine was introduced into the side chains of the oligomers. Fluorescent OFBT-A nanoparticles with good dispersibility were produced using the reprecipitation method, and DNA with attached TR dye (TR-DNA) could be loaded into the fluorescent OFBT-A nanocomposites without selectivity in the reprecipitation process. Efficient FRET was observed after the loading of sufficient amounts TR-DNA. The OFBT-A/TR-DNA nanocomposites showed good stability under the ionic strength in the solution environment and a wide working pH range. The capture abilities of the OFBT-A and the release process of the DNA were investigated by monitoring the FRET efficiency between OFBT-A and TR. In addition, the close-to-neutral surface and suitable size of the OFBT-A/TR-T5 nanocomposites resulted in enhanced internalization into A549 cells and a lower cytotoxicity compared with the OFBT-A nanoparticles. Short TR-DNA was also delivered into the cells, ensuring the good stability of the OFBT-A/TR-DNA composites. We therefore believe that these π-conjugated polymers or oligomers have great potential as a multifunctional siRNA delivery system, after further optimization and modification of their capabilities is performed.

ASSOCIATED CONTENT

Supporting Information

Emission spectra of OFBT-A in solutions with different THF/H_2O ratios (v/v), normalized absorption spectra for TR and emission spectra for OFBT-A in H_2O, normalized absorption of OFBT-A and OFBT-A/TR-T5, and excitation for OFBT-A/TR-T5 with emission at 525 nm. CLSM images of A549 cells untreated or incubated for 12 h with OFBT-A nanoparticles alone, TR-T5 alone, or OFBT-A/TR-T5 nanocomposites. This material is available free of charge via the Internet at http://pubs.acs.org.

AUTHOR INFORMATION

Corresponding Author

*E-mail: lidong@mater.ustb.edu.cn (Lidong Li); hefang@mater.ustb.edu.cn (Fang He).

Notes

The authors declare no competing financial interest.

■ ACKNOWLEDGMENTS

The authors gratefully acknowledge the financial support by the Program for New Century Excellent Talents in University of Ministry of Education of China (NCET-11-0576), the Fundamental Research Funds for the Central Universities of China.

■ REFERENCES

(1) Mulligan, R. C. *Science* **1993**, *260*, 926−932.
(2) Cavazzana-Calvo, M.; Hacein-Bey, S.; De Saint Basile, G.; Gross, F.; Yvon, E.; Nusbaum, P.; Selz, F.; Hue, C.; Certain, S.; Casanova, J. L.; Bousso, P.; Le Deist, F.; Fischer, A. *Science* **2000**, *288*, 669−672.
(3) Pack, D. W.; Hoffman, A. S.; Pun, S.; Stayton, P. S. *Nat. Rev. Drug Discovery* **2005**, *4*, 581−593.
(4) Yang, Z. R.; Wang, H. F.; Zhao, J.; Peng, Y. Y.; Wang, J.; Guinn, B.-A.; Huang, L. Q. *Cancer Gene Ther.* **2007**, *14*, 599−615.
(5) Elbashir, S. M.; Harborth, J.; Lendeckel, W.; Yalcin, A.; Weber, K.; Tuschl, T. *Nature* **2001**, *411*, 494−498.
(6) Dorsett, Y.; Tuschl, T. *Nat. Rev. Drug Discovery* **2004**, *3*, 318−329.
(7) Whitehead, K. A.; Langer, R.; Anderson, D. G. *Nat. Rev. Drug Discovery* **2009**, *8*, 129−138.
(8) Reischl, D.; Zimmer, A. *Nanomedicine* **2009**, *5*, 8−20.
(9) Sibley, C. R.; Seow, Y.; Wood, M. J. A. *Mol. Ther.* **2010**, *18*, 466−476.
(10) Akinc, A.; Zumbuehl, A.; Goldberg, M.; Leshchiner, E. S.; Busini, V.; Hossain, N.; Bacallado, S. A.; Nguyen, D. N.; Langer, R.; Anderson, D. G. *Nat. Biotechnol.* **2008**, *26*, 561−569.
(11) Heredia, K. L.; Nguyen, T. H.; Chang, C.-W.; Bulmus, V.; Davis, T. P.; Maynard, H. D. *Chem. Commun.* **2008**, 3245−3247.
(12) Howard, K. A. *Adv. Drug Delivery Rev.* **2009**, *61*, 710−720.
(13) Mintzer, M. A.; Simanek, E. E. *Chem. Rev.* **2009**, *109*, 259−302.
(14) Wagner, E. *Acc. Chem. Res.* **2012**, *45*, 1005−1013.
(15) Jeong, J. H.; Mok, H.; Oh, Y.-K.; Park, T. G. *Bioconjugate Chem.* **2009**, *20*, 5−14.
(16) Schroeder, A.; Levins, C. G.; Cortez, C.; Langer, R.; Anderson, D. G. *J. Intern. Med.* **2010**, *267*, 9−21.
(17) Han, L.; Zhao, J.; Zhang, X.; Cao, W.; Hu, X.; Zou, G.; Duan, X.; Liang, X. *ACS Nano* **2012**, *6*, 7340−7351.
(18) Tseng, Y.-C.; Mozumdar, S.; Huang, L. *Adv. Drug Delivery Rev.* **2009**, *61*, 721−731.
(19) Nuhn, L.; Hirsch, M.; Krieg, B.; Koynov, K.; Fischer, K.; Schmidt, M.; Helm, M.; Zentel, R. *ACS Nano* **2012**, *6*, 2198−2214.
(20) Hartono, S. B.; Gu, W.; Kleitz, F.; Liu, J.; He, L.; Middelberg, A. P. J.; Yu, C.; Lu, G.-Q.; Qiao, S.-Z. *ACS Nano* **2012**, *6*, 2104−2117.
(21) Biju, V.; Anas, A.; Akita, H.; Shibu, E. S.; Itoh, T.; Harashima, H.; Ishikawa, M. *ACS Nano* **2012**, *6*, 3776−3788.
(22) Alabi, C. A.; Love, K. T.; Sahay, G.; Stutzman, T.; Young, W. T.; Langer, R.; Anderson, D. G. *ACS Nano* **2012**, *6*, 6133−6141.
(23) Swager, T. M. *Acc. Chem. Res.* **1998**, *31*, 201−207.
(24) Chen, L.; McBranch, D. W.; Wang, H. L.; Helgeson, R.; Wudl, F.; Whitten, D. G. *Proc. Natl. Acad. Sci. U. S. A.* **1999**, *96*, 12287−12292.
(25) Wang, S.; Gaylord, B. S.; Bazan, G. C. *J. Am. Chem. Soc.* **2004**, *126*, 5446−5451.
(26) Liu, B.; Bazan, G. C. *Proc. Natl. Acad. Sci. U. S. A.* **2005**, *102*, 589−593.
(27) Thomas, S. W., III; Joly, G. D.; Swager, T. M. *Chem. Rev.* **2007**, *107*, 1339−1386.
(28) Feng, X. L.; Liu, L. B.; Wang, S.; Zhu, D. B. *Chem. Soc. Rev.* **2010**, *39*, 2411−2419.
(29) He, F.; Liu, L. B.; Li, L. D. *Adv. Funct. Mater.* **2011**, *21*, 3143−3149.
(30) Wang, X.; He, F.; Tang, F.; Li, L. *J. Mater. Chem.* **2012**, *22*, 15303−15308.
(31) Zhu, C.; Liu, L.; Yang, Q.; Lv, F.; Wang, S. *Chem. Rev.* **2012**, *112*, 4687−4735.
(32) Wu, C.; Bull, B.; Szymanski, C.; Christensen, K.; McNeill, J. *ACS Nano* **2008**, *2*, 2415−2423.
(33) Pecher, J.; Mecking, S. *Chem. Rev.* **2010**, *110*, 6260−6279.
(34) Tian, Z.; Yu, J.; Wu, C.; Szymanski, C.; McNeill, J. *Nanoscale* **2010**, *2*, 1999−2011.
(35) Wu, C.; Hansen, S. J.; Hou, Q.; Yu, J.; Zeigler, M.; Jin, Y.; Burnham, D. R.; McNeill, J. D.; Olson, J. M.; Chiu, D. T. *Angew. Chem., Int. Ed.* **2011**, *50*, 3430−3434.
(36) Wu, C.; Bull, B.; Christensen, K.; McNeill, J. *Angew. Chem., Int. Ed.* **2009**, *48*, 2741−2745.
(37) Petkau, K.; Kaeser, A.; Fischer, I.; Brunsveld, L.; Schenning, A. P. H. J. *J. Am. Chem. Soc.* **2011**, *133*, 17063−17071.
(38) Xu, X.; Chen, S.; Li, L.; Yu, G.; Di, C.; Liu, Y. *J. Mater. Chem.* **2008**, *18*, 2555−2561.
(39) Tang, F.; He, F.; Cheng, H.; Li, L. *Langmuir* **2010**, *26*, 11774−11778.
(40) Tang, F.; Ma, N.; Wang, X.; He, F.; Li, L. *J. Mater. Chem.* **2011**, *21*, 16943−16948.
(41) Wang, J.; Xu, X.; Zhao, Y.; Zheng, C.; Li, L. *J. Mater. Chem.* **2011**, *21*, 18696−18703.
(42) Cui, Q.; He, F.; Wang, X.; Xia, B.; Li, L. *ACS Appl. Mater. Interfaces* **2013**, *5*, 213−219.
(43) Feng, X.; Tang, Y.; Duan, X.; Liu, L.; Wang, S. *J. Mater. Chem.* **2010**, *20*, 1312−1316.
(44) Feng, X.; Yang, G.; Liu, L.; Lv, F.; Yang, Q.; Wang, S.; Zhu, D. *Adv. Mater.* **2012**, *24*, 637−641.
(45) Feng, X.; Lv, F.; Liu, L.; Tang, H.; Xing, C.; Yang, Q.; Wang, S. *ACS Appl. Mater. Interfaces* **2010**, *2*, 2429−2435.
(46) Silva, A. T.; Nguyen, A.; Ye, C. M.; Verchot, J.; Moon, J. H. *BMC Plant Biol.* **2010**, *10*, 291.
(47) Yang, G.; Lv, F.; Wang, B.; Liu, L.; Yang, Q.; Wang, S. *Macromol. Biosci.* **2012**, *12*, 1600−1614.
(48) Moon, J. H.; Mendez, E.; Kim, Y.; Kaur, A. *Chem. Commun.* **2011**, *47*, 8370−8372.
(49) Feng, X.; Lv, F.; Liu, L.; Yang, Q.; Wang, S.; Bazan, G. C. *Adv. Mater.* **2012**, *24*, 5428−5432.
(50) Philipp, A.; Zhao, X.; Tarcha, P.; Wagner, E.; Zintchenko, A. *Bioconjugate Chem.* **2009**, *20*, 2055−2061.
(51) Kim, H. J.; Ishii, A.; Miyata, K.; Lee, Y.; Wu, S. R.; Oba, M.; Nishiyama, N.; Kataoka, K. *J. Controlled Release* **2010**, *145*, 141−148.
(52) Ge, J.; Jacobson, G. B.; Lobovkina, T.; Holmberg, K.; Zare, R. N. *Chem. Commun.* **2010**, *46*, 9034−9036.
(53) He, C.; He, Q.; Deng, C.; Shi, L.; Fu, Y.; Cao, H.; Cheng, J. *Synth. Met.* **2011**, *161*, 293−297.
(54) Zhang, M.; Tsao, H. N.; Pisula, W.; Yang, C.; Mishra, A. K.; Müllen, K. *J. Am. Chem. Soc.* **2007**, *129*, 3472−3473.
(55) Abbel, R.; Weegen, R.; Meijer, E. W.; Schenning, A. P. H. J. *Chem. Commun.* **2009**, 1697−1699.
(56) Ku, S.-Y.; Chi, L.-C.; Hung, W.-Y.; Yang, S.-W.; Tsai, T.-C.; Wong, K.-T.; Chen, Y.-H.; Wu, C.-I. *J. Mater. Chem.* **2009**, *19*, 773−780.
(57) Li, Y.; Li, A.-Y.; Li, B.-X.; Huang, J.; Zhao, L.; Wang, B.-Z; Li, J.-W.; Zhu, X.-H.; Peng, J.; Cao, Y.; Ma, D.-G.; Roncali, J. *Org. Lett.* **2009**, *11*, 5318−5321.
(58) Wang, F. K.; Bazan, G. C. *J. Am. Chem. Soc.* **2006**, *128*, 15786−15792.
(59) Wang, L.; Pu, K.-Y.; Li, J.; Qi, X.; Li, H.; Zhang, H.; Fan, C.; Liu, B. *Adv. Mater.* **2011**, *23*, 4386−4391.
(60) Kaeser, A.; Fischer, I.; Abbel, R.; Basenius, P.; Dasgupta, D.; Gillisen, M. A. J.; Portale, G.; Stevens, A. L.; Herz, L. M.; Schenning, A. P. H. J. *ACS Nano* **2013**, *7*, 408−416.
(61) Lakowicz, J. R. *Principles of fluorescence Spectroscopy*, 3rd ed.; Springer Science, LLC: New York, 2006; p 960.
(62) Davis, M. E. *Mol. Pharmaceutics* **2009**, *6*, 659−668.
(63) Salvador-Morales, C.; Zhang, L.; Langer, R.; Farokhzad, O. C. *Biomaterials* **2009**, *30*, 2231−2240.